Int. Journal of Refractory Metals & Hard Materials 28 (2010) 377–382

Contents lists available at ScienceDirect

Int. Journal of Refractory Metals & Hard Materials

journal homepage: www.elsevier.com/locate/IJRMHM

# Microstructural characterization of Mo–12Si–8.5B alloy subjected to diffusion annealing treatment

S.P. Yang *, H. Kou, G.J. Zhang, G. Liu, F. Jiang, J. Sun

*State Key Laboratory for Mechanical Behavior of Materials, School of Material Science and Engineering, Xi'an Jiaotong University, Xi'an 710049, China*

ARTICLE INFO

*Article history:*
Received 2 September 2009
Accepted 2 December 2009

*Keywords:*
Mo–Si–B alloys
Microstructure
Diffusion annealing treatment

ABSTRACT

Microstructural evolutions in the solidification and subsequent diffusion annealing treatment of Mo–12Si–8.5B alloys have been studied by using XRD, OM, SEM and TEM. Because the annealing temperature (1900 °C) is in the vicinity of four-phase equilibrium eutectic reaction (1950 °C) point of L = $Mo_3Si$ + $Mo_5SiB_2$ ($T_2$)+$Mo_{ss}$ (Mo solid solution), the dendrites and lamellar phase have almost been dissolved. Dislocations, $Mo_{ss}$ precipitates and subgrain boundary have been observed in the $T_2$ phase while the other phases are not found. In addition, dislocations are from excess vacancy during the annealing treatment and play important roles for the $Mo_{ss}$ precipitate. The dislocations can serve as the heterogeneous nucleation sites and compose of sub-boundary which refines the grain size to some extent. The results observed in this study can be used as a reference for future work on the relationships between microstructure and mechanical property of the Mo–Si–B alloys.



## 1. Introduction

Mo–Si–B alloys are potentially significant materials for ultra-high temperature structural components because of their outstanding combination properties, such as high melting point, salient high temperature strength, low thermal expansion coefficient and excellent high temperature oxidation resistance [1]. At present, the main researches are centralized at the field of $Mo_{ss}$ (Mo solid solution) –$Mo_3Si$–$Mo_5SiB_2$ ($T_2$) with salient fracture toughness and easier to process [2,3]. $Mo_5SiB_2$ phase has attracted more attention because of its fascinating properties of nearly isotropic coefficients of thermal expansion, high moduli [4,5] and high temperature strength and oxidation resistance [6,7]. So the constitutional and lattice defect mechanism of the $T_2$ phase may be an important measure to consider and design the volume fraction in the multiphase alloys to achieve the optimization of mechanical properties.

Whereas many studies have been carried out on the microstructure characteristics in the multiphase Mo–Si–B alloys [3,7], little work is reported on the formation and movement of dislocation and polygonized structure after diffusion annealing in $Mo_{ss}$–$Mo_3Si$–$Mo_5SiB_2$ alloys so far. This work is aimed at investigating the solidification process and effect of diffusion annealing treatment on the microstructure and especially focused on the formation of $Mo_{ss}$ precipitates and relationship with matrix phase.

## 2. Experimental procedures

Alloys with nominal composition of Mo–12Si–8.5B (at.%) were prepared by using high purity elemental Mo (99.95 wt.%), Si (99.999 wt.%) and B (99.8 wt.%), which were added in bulk forms (small pieces) to promote striking arc and preventing splashing during the melting. The arc melting is in a partial pressure of Ar atmosphere (70 kPa). A pure Ti sample was melted more than five times before each melting cycle of Mo–12Si–8.5B alloys to deplete residual $O_2$ and $N_2$ present. The alloys remelted at least six times in order to obtain a chemical homogeneity because of the efficient diffusion in the melted condition. Then, arc-melted buttons with a total mass about 100 g were drop-cast into hemispheroidal water-cooled copper mould. These casts were subsequently annealed under a flow $H_2$ atmosphere for 60 h at 1900 °C, which is lower than four-phase equilibrium eutectic reaction point of 1950 °C.

Microstructural observation of the as-cast, heat-treated samples was carried by using optical metallography (OM) and scanning electron microscopy (SEM) with an energy dispersion spectrometer (EDS). These samples were firstly polished and then etched by Murakami's etching (an aqueous solution of 10 wt.% potassium ferricyanide and 10 wt.% sodium hydroxide). Phases in alloys and the changes in phases during the heat treatment were examined by X-ray diffraction. EDS was used to analyse the precipitate composition. In addition, the specimens for transmission electron microscopy (TEM) were fabricated by mechanical dimpling to near 30 μm thicknesses followed by ion milling using the Ar+ with the

* Corresponding author. Tel.: +86 13186143532.
*E-mail address:* yang_shuangping@yahoo.cn (S.P. Yang).

0263-4368/$ - see front matter © 2009 Elsevier Ltd. All rights reserved.
doi:10.1016/j.ijrmhm.2009.12.002

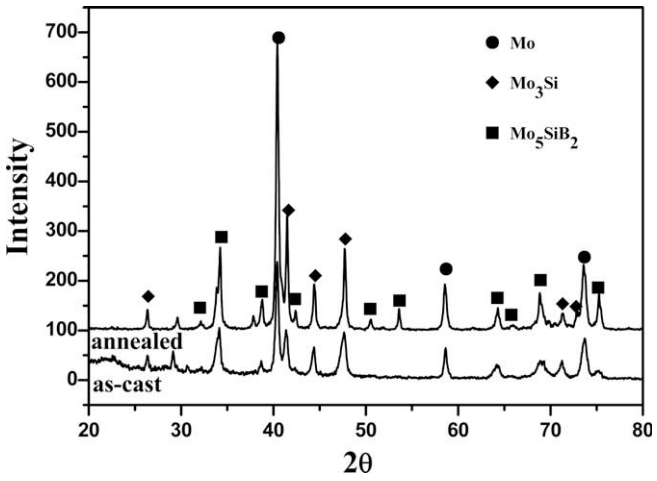


**Fig. 1.** XRD patterns of as-cast and annealed specimens indicating the consist of $Mo_{ss}$, $Mo_3Si$ and $Mo_5SiB_2$ and excess presence of $Mo_5SiB_2$ after the annealing treatment.

parameter of 5 kV and 5 mA. The indentation tests were performed at the load of 0.98 N and a loading time of 15 s.

## 3. Results and discussions

### 3.1. Phase composition and variation in the heat treatment of Mo–12Si–8.5B

Fig. 1 shows the X-ray diffusion patterns of as-cast and annealed samples, the nominal composition Mo–12Si–8.5B consists of $Mo_{ss}$, $Mo_3Si$ and $Mo_5SiB_2$. Compared with as-cast specimen, an excess couple of $Mo_5SiB_2$ peaks are present (such as 50.43°, 53.59° and 75.22°) and diffusion intensity of all phases are increased due to annealing temperature near the four-phase equilibrium reaction, which results in dramatic diffusion of elemental atoms to reach the homogeneous state. In previous papers [8,9], the authors have investigated that the non-equilibrium state are from mutual solid solution during the two or three phases eutectic reaction and the wide range of composition transition of $T_2$ phase. Through the efficient diffusion, the non-equilibrium state will be eliminated and the stable phase can be formed. The detailed annealed morphology and distribution will be particularly discussed later.

### 3.2. Solidification pathway and microstructure of the Mo–12Si–8.5B alloy

Fig. 2 shows the bulk dendrites mixing with a majority of finer lamellar phases under non-oriented solidification. Fig. 3 exhibits the liquid projection [10,11], the primary phase is $Mo_{ss}$ marked in black spot and go along the arrow line to the point of n in the eutectic trough between Mo and $Mo_5SiB_2$ via dendrite growth (Fig. 2(a)), which results in dendrite segregation proved by the microhardness and EDS. For instance, the mean hardness of dark dendrites is about 694HV0.1 lower than interdendritic composition near 3967HV0.1 and the element percents are also testified by the results of EDS. The scanning electron micrograph of as-cast with energy dispersion spectrometer is appeared in Fig. 2(b). The next solidification stage is co-precipitation of $Mo_{ss}/Mo_5SiB_2$ and the final step of solidification pathway is the ternary eutectic reaction of $L = Mo_3Si + Mo_5SiB_2 + Mo_{ss}$. In those solidification processes, volume fractions of eutectic phases play crucial roles on the mor-

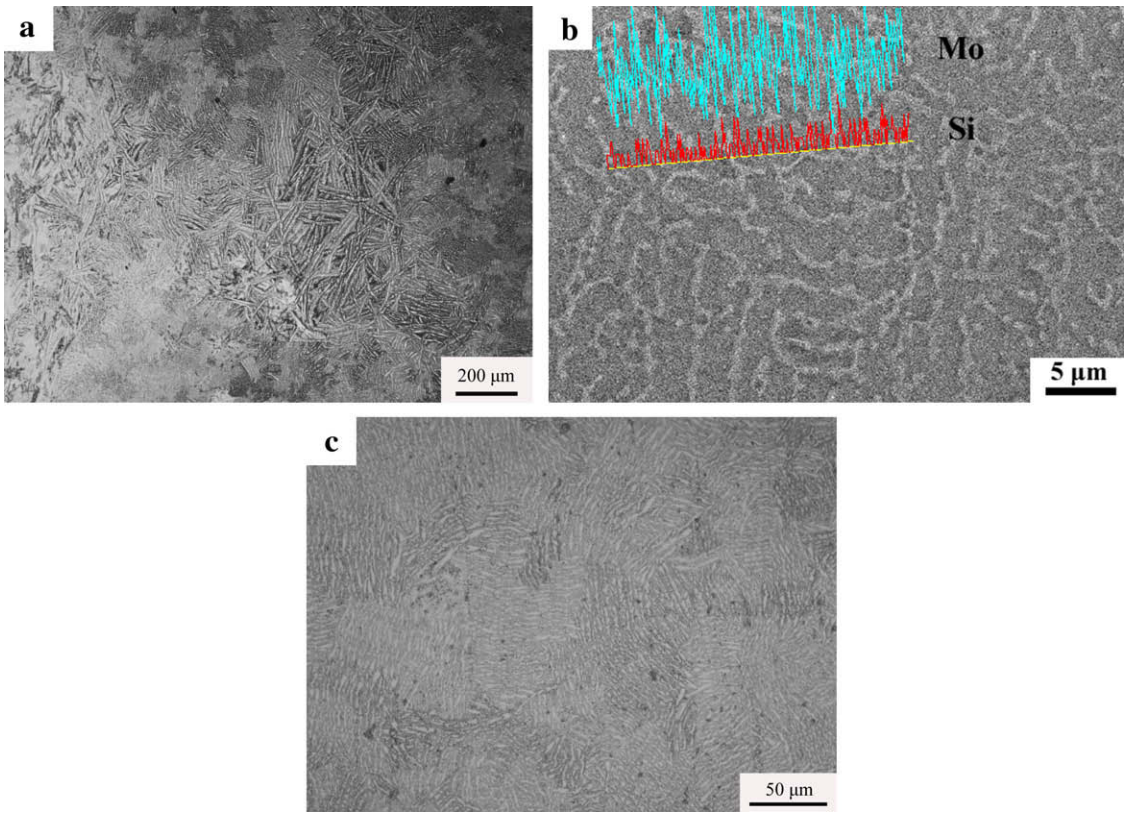


**Fig. 2.** Optical micrograph of Mo–12Si–8.5B (a) as-cast and (b) scanning electron micrographs of as-cast with energy dispersion spectrometer (c) optical micrograph of lamellar eutectics.

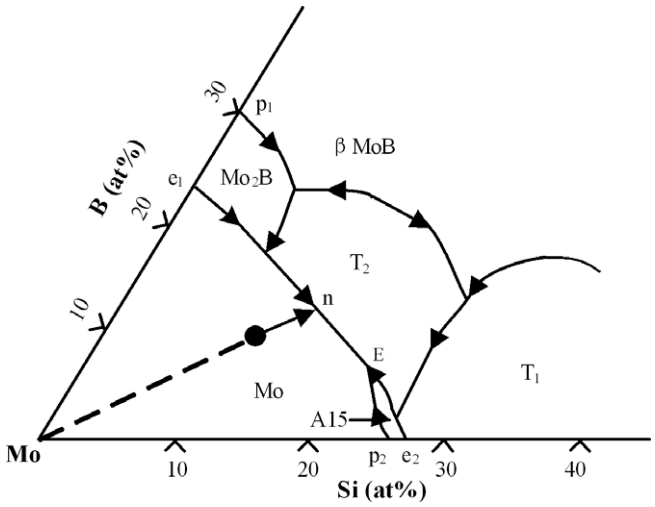


**Fig. 3.** Liquid projection on the Mo-rich portion of Mo–Si–B alloys. The black spot represents the composition of Mo–12Si–8.5B and dashed line exhibits the extension of solidification pathway for primary $Mo_{ss}$ [10].

phology and all transcend the volume fraction limitation of lamellar about $1/\pi$. The eutectic phases consist of lamellar structure with bridge joint growth and exhibit colour diversity owing to different orientations, as shown in Fig. 2(c).

### 3.3. Influence of diffusion annealing on microstructure

Fig. 4 shows the annealed microstructure of the alloy, the bright $Mo_{ss}$ is isolated by the dark intermetallic $Mo_3Si/T_2$ matrix and the annealed grains are well homogeneous as shown in the Fig. 4(a). The dendrite and lamellar structures are mostly dissolved but evidence of the cast microstructure clearly remains. For instance, a couple of intermetallics exhibit the inherited dendrites in Fig. 4(b). Due to sufficient diffusion of segregated elements during elevated temperature process, the annealed mean microhardness of bright $Mo_{ss}$ and dark matrix are about 550HV0.1 and 1661HV0.1, respectively, comparing with 694HV0.1 and 3967HV0.1 in the as-cast sample. In addition, the bright rod/needle-like precipitates

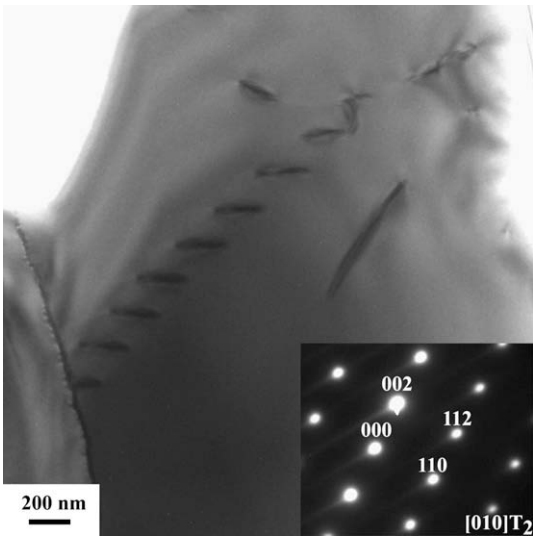


**Fig. 5.** TEM image showing dislocations in the $T_2$ phase in a sample annealed at 1900 °C for 60 h.

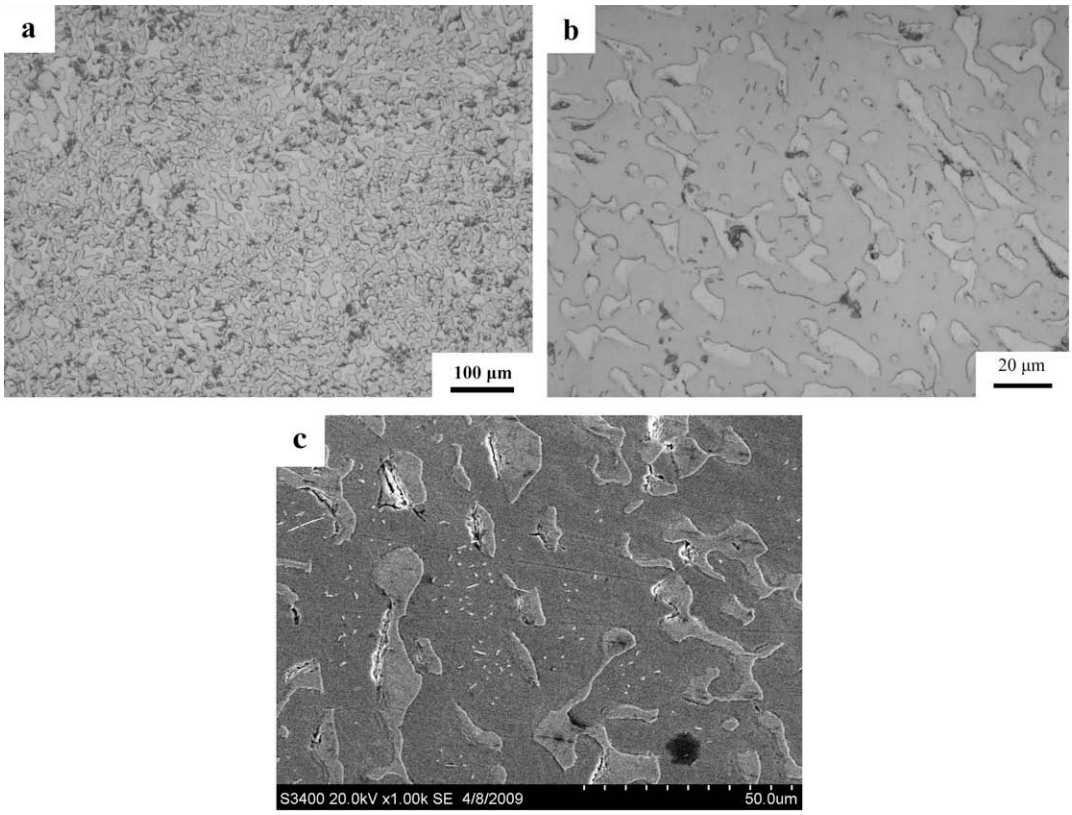


**Fig. 4.** Optical micrograph of annealed Mo–12Si–8.5B (a) and (b), (c) scanning electron micrographs of $Mo_{ss}$ precipitates after annealing treatment.

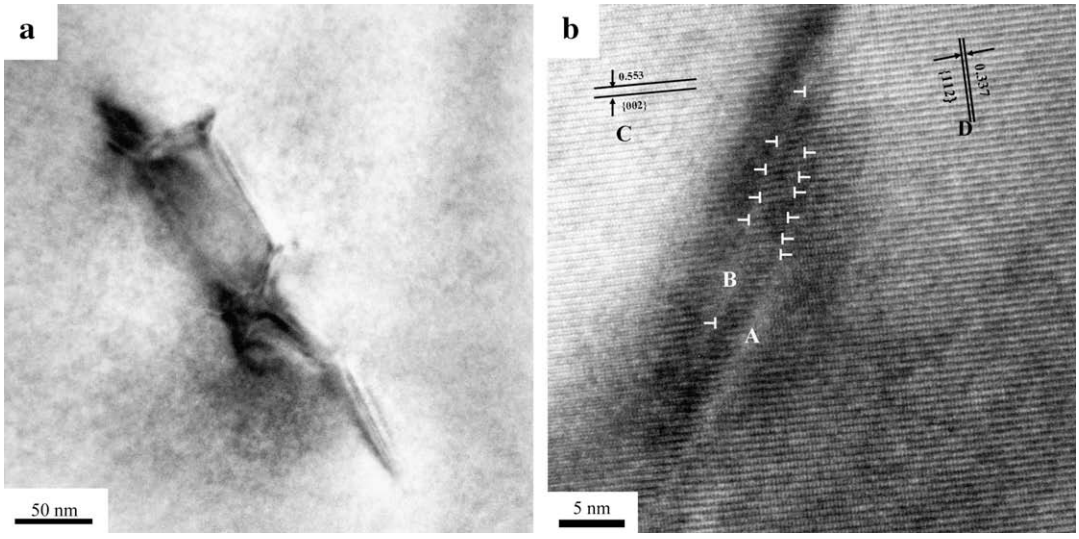


**Fig. 6.** (a) TEM bright field image of $Mo_{ss}$ precipitate within the $T_2$ matrix, (b) HRTEM image of $Mo_{ss}$ precipitate from the part of (a).

of $Mo_{ss}$ around 2–7 μm are dispersive distribution in the dark intermetallic matrix in Fig. 4(c). Nunes and Samadi et al. [12,13] have reported the effect of ductile-phase Mo, which can enhance the fracture toughness via the extrinsic toughening mechanisms such as ductile-phase bridging and microcracking mechanism. The effect of $Mo_{ss}$ precipitates on the toughness mechanism of

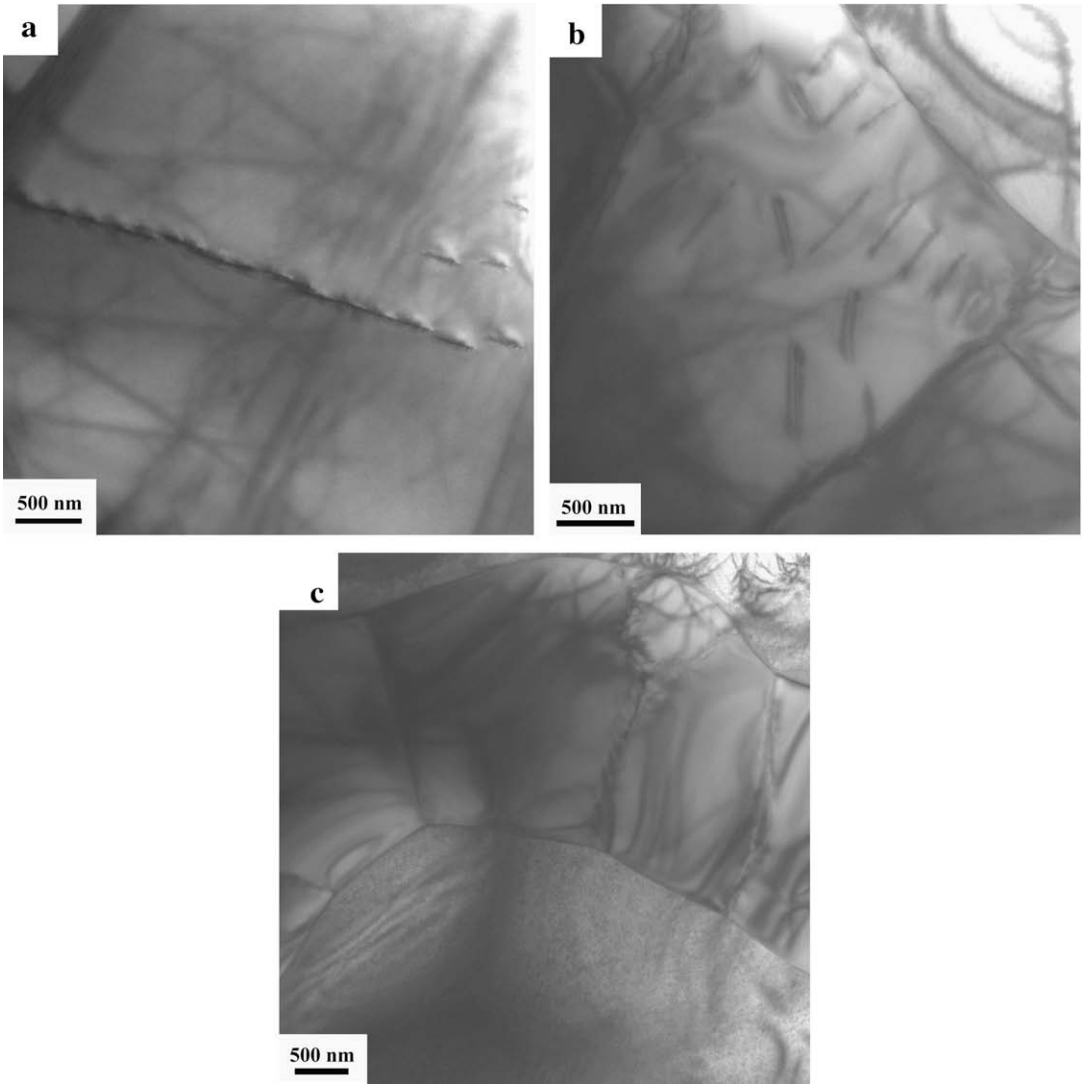


**Fig. 7.** TEM bright field image of $T_2$ matrix, (a) the dislocation wall, (b) polygonized structure from collapsed dislocation and (c) the formation of subgrain.

Mo–Si–B alloys is being systematically studied and will be reported in the future.

If the temperature of heating treatment is slight higher than the lowest eutectic temperature (1900 °C), the liquid phase will be present and the typical eutectic microstructure of petal-like morphology may be appeared because the slow cooling followed by furnace. In addition, parties of inherited dendrites may be effectively relived.

It is revealed from TEM observations that there are numerous dislocations within the $T_2$ phase (labelled in the lower right-hand area), as shown in Fig. 5, where of the dislocations found are almost straight ones in the same orientation at or near the interfaces. An explanation has been discussed by Sekido et al. [14], the reason for the nucleation of dislocation has been promoted by thermal stress at the interfaces and the interfaces can act as a sink of vacancies. Therefore, the dislocation has nucleated by thermal stress at or near the interface and can easily develop by absorbing a stream of excess vacancies flowing toward the interface.

Obviously, there is a tendency the appearances of dislocation are arranged in rows in Fig. 5. The later dislocation can eliminate the antiphase boundary from the former and recover ordered condition for the solid solution. And the spaces between the dislocations depend on the balance of antiphase boundary energy and repulsive force. This structure may enhance the strength of alloys. Field et al. [15] reported that the slip systems of dislocations in single phase $T_2$ are $\langle 1\,0\,0\rangle/\{0\,0\,1\}$ and $1/2\langle 1\,1\,1\rangle/\{1\,1\,2\}$. And those characters of dislocations in $T_2$ phase are related to alloys composition owing to dislocation's elastic energies.

In good agreement with the XRD patterns and SEM microstructures, there are numerous $Mo_{ss}$ precipitates and preferentially near dislocation within $T_2$ phase in Fig. 6(a). With the high energy of dislocations, the $Mo_{ss}$ precipitates preferentially nucleate on the dislocation, which are preferred $\langle 1\,1\,0\rangle$ to $\langle 1\,0\,0\rangle$ dislocations with the higher line energy stated by Nunes et al. [12].

The high-resolution TEM (HRTEM) image of $Mo_{ss}$ precipitate in Fig. 6(b) shows the coherences and partial semicoherences of $Mo_{ss}$ precipitates with the $T_2$ phase matrix. The interface between the $Mo_{ss}$ precipitates and $T_2$ matrix is low-angle grain boundaries and built by systematically arranged dislocations as marked with white lines, which generate long-range stress fields causing diffusion regions (see areas A and B). There are some bent lattice planes around the dislocation owing to the additionally introduced lattice plane in terms of stress areas.

The rod/needle-like morphology of $Mo_{ss}$ precipitates is intensely affected by the interfacial energy and elastic strain. And the interfacial energy is estimated by the atomic matching of the interface between the precipitate and the matrix. Hence, with the maximal appearance probability, the crystal nucleus should require minimal nucleation energy from salient matching relation. From the quantitative analysis of elastic strain energy, the most favourable morphology is lamellar shape, followed by rod and spherical shape in turn. On the other hand, the spherical morphology is optimal from interfacial energy [16]. Indeed, the morphology of precipitates is determined by the balance of elastic strain and interfacial energy. As depicted in Fig. 6(b), cross $\{0\,0\,2\}$ lattice fringes with a lattice spacing about 0.553 nm (see C) and $\{1\,1\,2\}$ lattice fringes with a spacing about 0.337 nm (see D), are apparent observed.

As shown above, some annealed microstructures are even finer than cast eutectic microstructure in Fig. 2. Unlike the alloys through the cold-work, the driving force of diffusion energy is from the long time annealing treatment at high temperature and segregated elements are sufficient to diffuse and develop the phase with new morphology. Simultaneously, homogeneous dislocations are moving and arraying via climb motion from the level to vertical combination, which result in formation of dislocation wall within $T_2$ phase in Fig. 7(a) and segregation of bulk alloys can be relieved. Furthermore, the formation of polygonized structure is constituted by dislocation walls and also termed subgrain structure in Fig. 7(b). In fact, the processing of polygonization is from high energy confusion condition to low energy regulation, which lead to the crystal integrity with lower dislocation density inner grain and significantly decreased the internal stress. Fig. 7(b) and Fig. 7(c) shows the equiaxed subgrain with size of approximately several microns can effectively refine the large eutectic structure. The polygonized structure with around equiaxial shape is the feature of in situ recrystallization, which did not rely on the storage power of cold-work but driven by long time annealing treatment.

## 4. Conclusion

The current investigation demonstrates the solidification pathway and morphology and the influence of diffusion annealing on Mo–12Si–8.5B alloys. The primary dendrites and lamellas of eutectic intermetallics are almost dissolved and parts of are spheroidized. After the long time annealing at high temperature, the mean microhardness of the $Mo_{ss}$ and the intermetallic matrix are from 694HV0.1 and 3967HV0.1 to 550HV0.1 and 1661HV0.1, respectively. And a rod/needle-shaped $Mo_{ss}$ precipitates about several microns are precipitated around the dislocations that are from high density vacancies and act as the heterogeneous nucleation sites. The interfacial relationship between $Mo_{ss}$ precipitates and $T_2$ matrix are mostly coherent or partially semicoherent. Simultaneously, homogeneous dislocations are climbed motion and arrayed to develop vertical combination resulting in formation of dislocation wall and polygonized structure within $T_2$ phase and the other phases are not found out.

## Acknowledgements

This work was supported by the National Natural Science Foundation of China (50801051) and National High Technology Research and Development Program of China (Grant No. 2008AA031001). The authors also wish to express their special thanks for the supports from the State Key Laboratory for Mechanical Behavior of Materials and Jinduicheng Molybdenum Co., Ltd. of China.

## Reference

[1] Akinc M, Meyer, Kramer MJ, Thom AJ, Huebsch JJ, Cook B. Boron-doped molybdenum silicides for structural applications. Mater Sci Eng A 1999;261:16–8.
[2] Huebsch JJ, Kramer MJ, Zhao HL, Akinc M. Solubility of boron in $Mo_{5+y}Si_{3-y}$. Intermetallics 2000;8:143–50.
[3] Sakidja R, Wilde G, Sieber H, Perepezko JH. The formation of Mo precipitates in a supersaturated $Mo_5SiB_2$ intermetallic phase. Philos Mag Lett 1999;79:351–7.
[4] Ito K, Ihara K, Tannka K, Fujikura M, Yamaguchi M. Physical and mechanical properties of single crystals of the $T_2$ phase in the Mo–Si–B system. Intermetallics 2001;9:591–602.
[5] Ihara K, Ito K, Tannka K, Yamaguchi M. Mechanical properties of $Mo_5SiB_2$ single crystals. Mater Sci Eng A 2002;222:329–31.
[6] Ito K, Kumagai M, Hayashi T, Yamaguchi M. Room temperature fracture toughness and high temperature strength of $T_2/Mo_{ss}$ and (Mo, Nb)$_{(ss)}/T_1/T_2$ eutectic alloys in the Mo–Si–B system. Scr Mater 2003;49:285–90.
[7] Kim S, Sakidja R, Perepezko JH, Kim YW. In: MRS symposium proceedings, vol. 646. Warrendale: MRS; 2001. p. N5. 42.1.
[8] Schneibel JH, Liu CT, Easton DS, Carmichanel CA. Microstructure and mechanical properties of Mo–$Mo_3Si$–$Mo_5SiB_2$ silicides. Mater Sci Eng A 1999;1–2:78–83.
[9] Sakidja R, Perepezko JH, Kim S, Sekido N. Phase stability and structural defects in high-temperature Mo–Si–B alloys. Acta Mater 2008;56:5223–44.
[10] Kim S, Perepezko JH. Interdiffusion kinetics in the $Mo_5SiB_2$ ($T_2$) phase. J Phase Equilib Diffus 2006;27:605–13.
[11] Ritchie RO, Zhang XF, De-Jonghe LC. On the role of grain-boundary films in optimizing the mechanical properties of silicon carbide ceramics. Int J Fracture 1999;100:58–83.
[12] Nunes CA, Sakidja R, Dong Z, Perepezko JH. Liquidus projection for the Mo-rich portion of the Mo–Si–B ternary system. Intermetallics 2000;8:327–37.

[13] Samadi A, Abdollah-zadeh A, Behrouzghaemi S, Razavi SH. Effect of solid solution supersaturation on precipitation of $\gamma'$ in rapidly quenched Ni–Al binary alloys. J Mater Sci Technol 2009;25:130–4.
[14] Sekido N, Sakidja R, Perepezko JH. Annealing response of point defects in off-stoichiometric $Mo_5SiB_2$ phase. Intermetallics 2007;15:1268–76.
[15] Field RD, Thoma DJ, Cooley JC, Chu F, Fu CL, Yoo MH, et al. Dislocations in $Mo_5SiB_2$ ($T_2$) phase. Intermetallics 2001;9:863–8.
[16] Ko HS, Paik KW, Park LJ, Kim YG, Tundermann JH. Influence of rhenium on the microstructures and mechanical properties of a mechanically alloyed oxide dispersion-strengthened nickel-base superalloy. J Mater Sci 1998;33:3361–70.